

Data Compression and Covariance Matrix Inspection: Cosmic Shear

Tassia Ferreira^{1,2}, Tianqing Zhang¹, Nianyi Chen¹, Scott Dodelson¹

¹*Department of Physics, Carnegie Mellon University, Pittsburgh, Pennsylvania 15312, USA*

²*PPG Cosmo, Universidade Federal do Espírito Santo,*

Avenida Fernando Ferrari 514, 29075-910 Vitória, Espírito Santo, Brazil

(LSST Dark Energy Science Collaboration)

(Dated: March 9, 2020)

In this paper, we start along the path of comparing covariance matrices for cosmic shear statistics generated by two different codes. The main goal is to identify the parts of the covariance matrix that are most significant to parameter estimation, and therefore which ones should be calculated more accurately. We engage different ways of doing this, starting with a simple one-to-one comparison of the elements, then moving on to eigenvalues and finally to the signal-to-noise ratio (SNR). In the spirit of reducing the number of relevant elements, we remove 200 modes associated with the highest eigenvalues, then those with the lowest SNR. We find that it is not possible to locate the most important elements using the first method but, while the analysis with the SNR proved resourceful for a few parameters of interest, like Ω_m , we lost constraining power on the intrinsic alignment (IA) parameters as well as S_8 . We also tested ways to shrink the covariance matrix, both at the tomographic level, and for the two-point functions. The former was accomplished using a method based on the Karhunen-Loève (KL) decomposition to obtain the modes with highest SNR, and we show that, in order to reproduce compatible results, we need at least two KL-modes, but just like in the SNR case, this is not the case for all parameters. Finally, we apply a lossless compression scheme to the covariance matrix, capable of reducing the dimension to the number of free parameters. We were successful in reproducing the constraints obtained previously and show that the elements of the new matrix have an error tolerance of up to 25%.

I. INTRODUCTION

Cosmic shear is a weak lensing effect caused by the large-scale structure of the universe, and is an important tool for constraining cosmology. Here, we will deal with its covariance matrix, which is an essential component in the analysis of the cosmic shear data. For a data vector of length N , the covariance matrix is a symmetric $N \times N$ matrix with $N \times (N + 1)/2$ individual elements that capture the auto and cross-correlation of the data vector. As data sets increase, the number of elements in the covariance matrix grows quadratically and becomes harder to analyse. In this paper, we will focus on cosmic shear measurements from the Dark Energy Survey (DES) [17] Year 1 release; the data vector has 227 elements, varying with angular separation, and different pairs of tomographic redshift bins. In this case, then, the number of independent elements of the covariance matrix is 25,878.

There are multiple codes that are able to generate the cosmic shear covariance matrix. In particular, we are considering two of them [13] [12], which will be discussed in detail in §II.

In this paper, we are trying to achieve the following goals:

- Among the vast number of elements in the covariance matrix, identify the most important ones.
- Explore methods to shrink the covariance matrix.
- Introduce noise to the elements in order to test their tolerance by quantifying responses in the likelihood analysis.

We accomplish these by considering several methods of identifying the elements of the covariance matrix that are most relevant. In §II, we describe the data set and the pair of covariance matrices used. The next three sections walk through increasingly complex ways of determining the most important parts of these matrices: we start with an element by element comparison of the two covariance matrices in §III, then move on to look at the eigenvalues in §IV, and, finally we use the signal-to-noise ratio in §V. We validate our findings by comparing them with the constraints obtained with the unmodified covariance matrix.

A simple compression method is applied in both §IV and V, where we discard 200 modes of the covariance matrix associated with the highest eigenvalues, then those with lowest signal-to-noise ratio, respectively. We apply more complicated compression schemes in §VI, using techniques developed by Alonso [2] and by Tegmark and Heavens [16], capable of reducing the dimension to the number of free parameters, thus obtaining a compression ratio of 1%. Our tolerance test is described in §VII, where we compare what happens to the parameter constraints when we introduce noise to elements and eigenvalues separately. Finally, our conclusions are summarised in §VIII.

II. DES COSMIC SHEAR: DATA AND ANALYSIS

In this section, we introduce the data and covariance matrices that are used in this work. Our tests are carried out using cosmic shear statistics $\xi_{\pm}(\theta)$, focusing on

Parameter	Prior
Cosmological	
Ω_m	$\mathcal{U}(0.1, 0.9)$
$\log A_s$	$\mathcal{U}(3.0, 3.1)$
$H_0(\text{kms}^{-1}\text{Mpc}^{-1})$	$\mathcal{U}(55, 91)$
Ω_b	$\mathcal{U}(0.03, 0.07)$
$\Omega_\nu h^2$	$\mathcal{U}(0.0005, 0.01)$
n_s	$\mathcal{U}(0.87, 1.07)$
Astrophysical	
A	$\mathcal{U}(-5, 5)$
η	$\mathcal{U}(-5, 5)$
Systematic	
m^i	$\mathcal{G}(0.012, 0.023)$
Δz^1	$\mathcal{G}(-0.001, 0.016)$
Δz^2	$\mathcal{G}(-0.019, 0.013)$
Δz^3	$\mathcal{G}(0.009, 0.011)$
Δz^4	$\mathcal{G}(-0.018, 0.022)$

TABLE I. List of the priors used in the analysis for parameter constraints (\mathcal{U} denotes flat in the given range and \mathcal{G} is gaussian with mean equal to its first argument and dispersion equal to its second). For the cosmological parameters, we fix $w = -1.0$, $\Omega_k = 0.0$ and $\tau = 0.08$. The astrophysical parameters are associated with the intrinsic alignment, they follow the relation $A(z) = A[(1+z)/1.62]^\eta$. Lastly, for systematics we have m^i corresponding to the shear calibration and Δz^i for the source photo- z shift, with $i = 1, 4$ in both cases.

the Year 1 results of the Dark Energy Survey [1, 17] (DESY1). The data is divided into four tomographic redshift bins spanning the interval $0.20 < z < 1.30$, which yields 10 bin-pair combinations, each one containing 20 angular bins between 2.5 and 250 arcmin. We thus begin with 200 data points for each $\xi_+(\theta)$ and $\xi_-(\theta)$, giving 400 in total. We then apply the angular cuts described in [1], which removes the scales most sensitive to baryonic effects; this leaves 167 points for $\xi_+(\theta)$ and 60 for $\xi_-(\theta)$, resulting in 227 data points corresponding to the aforementioned 227×227 covariance matrix.

Table I shows the 16-parameters varied and the priors placed on them. To perform cosmological parameter inference we use the **CosmoSIS** [3, 5, 8, 10, 11, 14, 15, 19] pipeline, while employing the **MultiNest** [6] sampler to explore the parameter space, with 1000 **livepoints**, **efficiency** set to 0.05, **tolerance** to 0.1 and **constant efficiency** set to True.

The covariance matrices used are the following:

- one obtained using **Cosmolike** [13] (CL), which was also used in the initial DESY1 analysis;
- one containing only the Gaussian part, obtained by running the same code used to analyse the KiDS-450 survey [12], using DESY1 parameters and to-

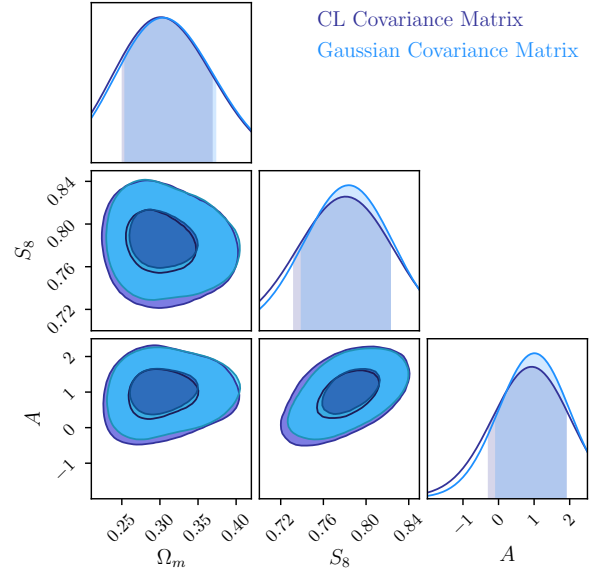


FIG. 1. Constraints on cosmological parameters Ω_m and S_8 and intrinsic alignment parameter A for two covariance matrices produced for cosmic shear. The purple curve is for CL while the blue is for the Gaussian. In the 16 parameter space, the volume of the posterior is about 22% larger for the former.

mographic bins. We refer to it simply as the Gaussian covariance matrix.

Thus, throughout, the covariance labels CL and Gaussian differ for several reasons: first, they are two independent codes and, second, although the code for the KiDS-450 survey does contain all the functionality in CL, we ran with the simplest settings in order to accentuate the differences. The ensuing larger differences will help us assess various validation techniques. Where not otherwise stated, the analysis and constraints will be performed on the CL covariance matrix.

Figure 1 shows the results for the projected cosmological constraints for CL. These projections use the same data vector and cuts, but the two different covariance matrices. The 2σ constraints are as follows: for CL: $\Omega_m = 0.306^{+0.073}_{-0.060}$, $A = 0.852^{+1.005}_{-1.086}$ and $S_8 = 0.784^{+0.200}_{-0.171}$; and for the Gaussian one: $\Omega_m = 0.309^{+0.073}_{-0.058}$, $A = 0.948^{+0.916}_{-0.985}$ and $S_8 = 0.787^{+0.196}_{-0.166}$. This shows that the differences we have introduced to the calculation of the two matrices are measurable in the parameter constraints.

III. ELEMENT-BY-ELEMENT COMPARISON

In this section, we perform an element-by-element comparison between the two covariance matrices. If there were only a single data point, then the covariance matrix would be one number and comparing two covariance matrices to try to understand why they give different constraints would be as simple as comparing these two

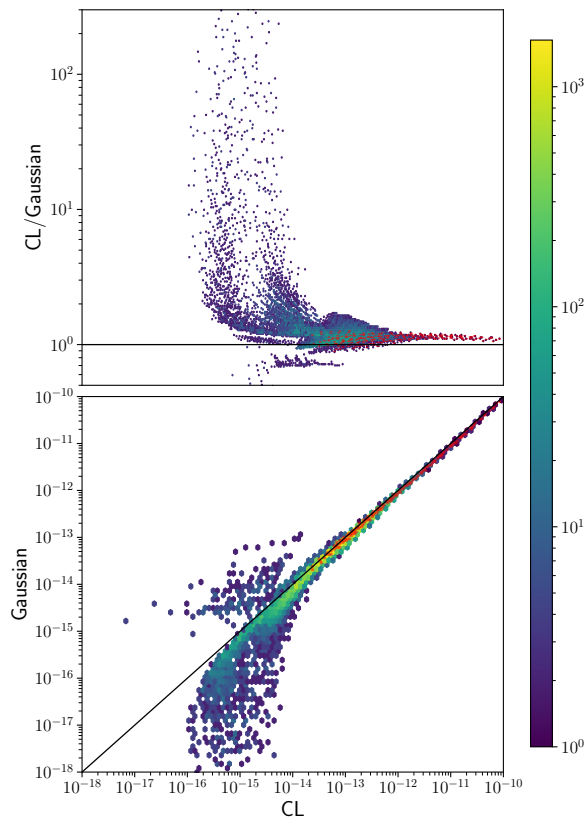


FIG. 2. In both plots, the red points refer to the diagonal elements, and the colour bar varies according to the number of elements in one hexagonal bin, where the darkest blue colour corresponds to only one element, and the brightest yellow shade to 2000. **Top:** Scatter plot of the ratio of the elements of CL and the Gaussian one vs the Gaussian value. For illustrative purposes, we draw a black, horizontal line at $CL/Gaussian = 1$. **Bottom:** Density of the scatter plot of the positive elements of the covariance matrices Gaussian and CL, with the black line showing $x = y$.

numbers. The simplest generalisation is then to do an element-by-element comparison. We make a scatter plot of the elements of the two matrices in the bottom panel of Figure 2, where we can see that the elements of CL are, in general, larger than the Gaussian's, differing by up to 4 orders of magnitude. In some ways, this is useful and reassuring, as it aligns with what we see in the parameter constraints, in Figure 1: larger elements in the covariance matrix translates to less constraining power.

The limitation of this method is that it remains unclear which of the differences are driving the final discrepancies in parameter constraints. This difficulty is an outgrowth of the increasing size of the data sets and hence the growing number of elements of the covariance matrix that any two codes are likely to disagree on. This element-by-element comparison, however, would prove much more useful if we could first determine the important elements. Towards that end, we start by turning to the eigenvalues.

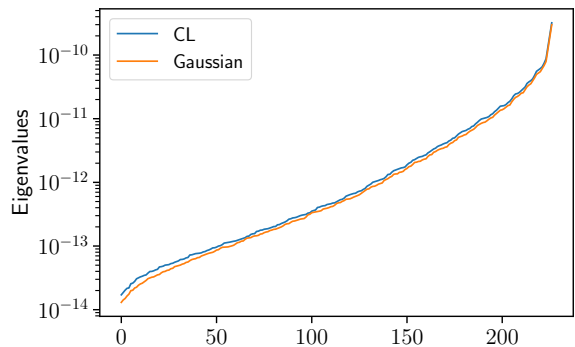


FIG. 3. A log plot showing the 227 eigenvalues of CL (blue) and the Gaussian (orange) covariance matrices.

IV. EIGENVALUES

The next attempt is to explore the eigenvalues of the covariance matrix. Each eigenvalue is associated with a linear combination of the data vector, or a *mode*, and it is possible that identifying the modes that have the most discrepant eigenvalues will give guidance on how to reconcile differences. We plot the eigenvalues for these matrices in Figure 3. At a first glance, both curves show reasonable agreement, with values differing only by an average of $\approx 13\%$.

The lowest eigenvalues correspond to modes with the smallest variance but since they are not normalised, it is unclear how this variance compares to the signal in the mode. Let us nonetheless explore the possibility that the modes with the lowest variance provide the most information and therefore dropping the ones with the largest eigenvalues would not affect the final result.

Our procedure consists of first diagonalising the covariance matrix in order to calculate its eigenvalues and then replacing the large eigenvalues with a larger number (nine orders of magnitude higher), thus removing their effective contribution; we then transform back to the original basis and perform a cosmological analysis with the new covariance matrix, to constrain the parameters of our model.

Figure 4 shows the results obtained after discarding the 200 eigenmodes with the largest eigenvalues by following the method described above. The constraints are significantly broader for the three parameters shown. This is consistent with the fact that we are throwing away about 90% of the information. However, it is inconsistent with the notion that these modes are irrelevant, in fact, constraints on $S_8 \equiv \sigma_8(\Omega_m/0.3)^{0.5}$ for the original covariance matrix are $0.784^{+0.200}_{-0.171}$, whereas, for this procedure, we obtain $0.679^{+0.533}_{-0.505}$, showing an increase in almost 200%. It is then clear that a different way of ordering the modes, other than simply looking at the eigenvalues, is called for.

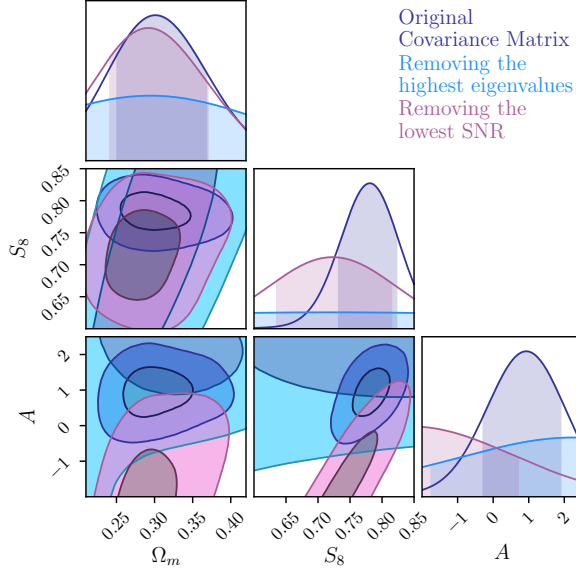


FIG. 4. Constraints on cosmological parameters Ω_m , S_8 and the intrinsic alignment parameter A for the original CL covariance matrix (in purple) and for two new covariance matrices obtained by setting the 200 highest eigenvalues of the original matrix to nine orders of magnitude higher (in blue), and by replacing the 200 lowest values of the SNR to seven order of magnitude lower (in magenta).

V. SIGNAL-TO-NOISE RATIO

Instead of looking only at the “noise” – or the eigenvalues of the covariance matrix – a better way to assess the importance of modes is to consider the signal as well. We can define the expected signal-to-noise ratio (SNR) as

$$\left(\frac{S}{N}\right)^2 = \sum_{ij} T_i C_{ij}^{-1} T_j, \quad (1)$$

where T_i and T_j are the predicted theoretical signal for the i^{th} data point and C is the covariance matrix. If C were diagonal, then the eigenvectors would simply be the data points themselves, and we could estimate the SNR squared expected in each mode by just computing T_i^2/C_{ii} . Then we could throw out the modes with the lowest SNR. Since C is not diagonal, we have to first diagonalise it and then order the values. So, we write the expected SNR squared as

$$\left(\frac{S}{N}\right)^2 = \sum_i \frac{v_i^2}{\lambda_i}, \quad (2)$$

where λ_i are the eigenvalues of the covariance matrix, which is diagonalised with the unitary matrix U , and the eigenvectors are

$$v_i \equiv U_{ij}^T T_j. \quad (3)$$

This makes it very clear which modes should be kept and which should be dropped. Modes v_i for which v_i^2/λ_i is very small can be discarded.

After obtaining the SNR for the covariance matrix, we proceed to set the 200 lowest values to seven orders of magnitude lower, which is equivalent to increasing the noise (or decreasing the signal) of these modes. We then obtain a new covariance matrix with the corresponding modified SNR values.

The parameter constraints for this method are shown in Figure 4, where we note that only Ω_m is well constrained (in agreement with those obtained with the original covariance matrix to within a 2σ interval). The constraining power on A and S_8 , on the other hand, is very much lost, which suggests that the modes removed do indeed carry relevant information for these parameters.

We can investigate this loss by tweaking our understanding of which modes carry information. The “signal” these modes are ordered by is the amplitude of the data points. The parameters, however, are sensitive to the shape as well as the amplitude. To address this, we can identify the SNR for each parameter individually by taking

$$\left(\frac{\partial S/\partial p_\alpha}{N}\right)^2 = \sum_i \frac{(\partial v_i/\partial p_\alpha)^2}{\lambda_i} \quad (4)$$

where $\partial/\partial p_\alpha$ is the derivative with respect to each parameter. This produces the SNR for each parameter of interest. The importance of this procedure is illustrated in Figure 5, which shows the normalised vanilla SNR for a given mode on the x -axis and the SNR for each parameter for the same mode, for brevity, we show only for Ω_m and A . The shaded region is the one excluded in the previous analysis, but clearly there are some low SNR modes there that contain information about the parameters. This is particularly true for the intrinsic alignment parameter A , which seems to explain the poor constraints shown in Figure 4. As a result, simply cutting on raw SNR loses constraining power.

VI. SHRINKAGE

Since the simplest methods of identifying the most relevant modes are imperfect, we turn to more sophisticated methods [7, 9, 16] that have been shown to reduce the number of modes significantly while preserving the cosmological information. First, there is compression at the ℓ -space [2], where linear combinations of the tomographic maps are used to retain as much information as possible. Compression of the tomographic bin-pairs then considerably reduces the size of the data vector of two-point functions. For example, we will see that most of the information in the four tomographic bins used by DESY1 can be compressed into a single linear combination of those bins. Therefore, instead of $(4 \times 5)/2$ two-point functions for each angular bin, we need include only one:

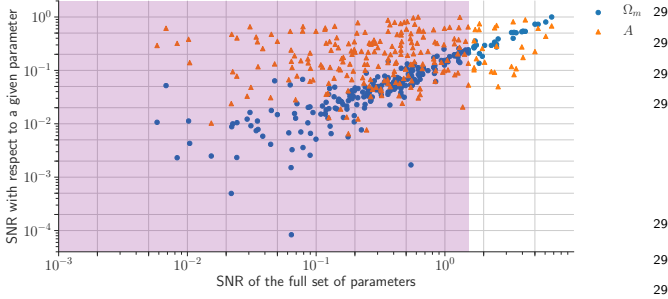


FIG. 5. Scatter plot for the relation between the signal to noise obtained with the covariance matrix for CL for each parameter (x-axis) against that for the full set of parameters (y-axis). The derivatives are shown with respect to Ω_m (blue circle) and for the intrinsic alignment parameters A (orange triangle). The purple rectangle spreads until the two hundredth lowest value of SNR, which corresponds to the values that are modified for parameter constraints.

the compression in the size of the data vector by a factor of ten means that there are a hundred fewer elements of the covariance matrix to study.

The second method directly operates on the two-point functions themselves [18], where the modes used are those that maximise the Fisher information for each of the cosmological parameters. Here, the size of the data vector is just the number of parameters used to fit the data (i.e. sixteen), so the compression eliminates even more modes than the tomographic compression. Roughly speaking, the numbers are the same: a data vector reduced by a factor of ten and the number of elements in the covariance matrix reduced by a factor of a hundred.

A. Tomographic Compression

This compression method is based on Karhunen-Loève (KL) decomposition for the shear power spectrum suggested by [2] and later applied to real space two-point function in [4] for CFHTLens survey. This method generally finds the eigenmode with most of the signal-to-noise ratio contribution to the power spectrum, and then transforms the two-point function in real space based on this eigenmode.

With CosmoSIS, we can generate the shear power spectrum C_ℓ^{ij} of convergence $a_{\ell m}$ for a fiducial cosmology. The cosmology we choose is the best-fit value of the DES Year 1 results for cosmic shear only. With the shear power spectrum $C_\ell = S_\ell + N_\ell$ and its shape noise N_ℓ , we can calculate the Karhunen-Loève (KL) modes matrix E_ℓ^{ij} via a general eigenvalue problem

$$C_\ell^{ij} E_\ell^j = \lambda_\ell^i N_\ell^{ij} E_\ell^j. \quad (5)$$

Each row in E_ℓ corresponds to a KL-mode of C_ℓ . Using the Cholesky decomposition, $N_\ell = LL^\dagger$, the new observable can be expressed as $b_{\ell m} = E_\ell \cdot L^{-1} a_{\ell m}$. We should

note that C_ℓ is the angular power spectrum of the weak lensing shear, and E_ℓ is similar to a transformation of basis for the shear. So, we can now calculate the power spectrum D_ℓ for the new observable $b_{\ell m}$

$$D_\ell = \langle b_{\ell m} b_{\ell m}^T \rangle = E_\ell L^{-1} C_\ell L^{-1} E_\ell^T, \quad (6)$$

or, if we denote $E_\ell N^{-1}$ as R_ℓ and further denote $U_\ell^{ij} = R_\ell^i R_\ell^j$, we can write the compression in one simple linear combination of the C_ℓ ,

$$D_\ell = R_\ell^i C_\ell^{ij} R_\ell^j = U_\ell^{ij} C_\ell^{ij}. \quad (7)$$

The double summation U_ℓ^{ij} is a weight on the tomographic bin-pair, which we can later use to compress the two-point functions. We should point out that these KL-modes are uncorrelated, so the power spectrum of the new observable D_ℓ is a diagonal matrix, with $1+\text{SNR}$ of the corresponding eigenmodes on the diagonal elements. Since the KL-decomposed modes of shear power spectrum are uncorrelated, we can make a compression here by taking only the first one or two modes with the highest SNR. By doing so, we compress ten tomographic bin-pairs to one or two.

We want, however, to eventually compress the two-point function data vector of DESY1. One possible way is to calculate the two-point function of the KL mode of the shear power spectrum,

$$\xi_\pm^{ij}(\theta) = \int \frac{\ell d\ell}{2\pi} J_{0/4}(\ell\theta) C_\ell^{ij}(\ell). \quad (8)$$

In order to compress ξ_\pm based on the compression of the C_ℓ , we need to make sure that our scheme is ℓ -independent, that is to say, the two-point correlation function of D_ℓ , $\tilde{\xi}_\pm(\theta)$, can be directly calculated from other two-point functions. We then have,

$$\begin{aligned} \tilde{\xi}_\pm(\theta) &= \int \frac{\ell d\ell}{2\pi} J_{0/4}(\ell\theta) D_\ell(\ell) \\ &= \int \frac{\ell d\ell}{2\pi} J_{0/4}(\ell\theta) U_\ell^{ij} C_\ell^{ij}(\ell) \\ &= U_\ell^{ij} \xi_\pm^{ij}(\theta), \end{aligned} \quad (9)$$

where U_ℓ^{ij} , the ℓ -independent compression weight is given by

$$U_\ell^{ij} = \frac{\int_{\ell_{\min}}^{\ell_{\max}} (2\ell + 1) U_\ell^{ij}}{\int_{\ell_{\min}}^{\ell_{\max}} (2\ell + 1)}. \quad (10)$$

We make a more conservative angular cut than the one discussed in [17], making sure that both ξ_\pm are uniform in regard to tomographic combinations. We consider an angular scale for ξ_+ from 7.195° to 250.0° , and for ξ_- from 90.579° to 250.0° . Therefore, for the purpose of demonstrating KL-transform, the raw data vector has a length of 190, and by shrinking 10 tomographic combinations for each angle into 1 KL-mode, the data is shrunk

to 19, and so the number of elements in the covariance matrices are reduced by 99%.

With **CosmoSIS**, we calculate the shear power spectrum C_ℓ of DES Year 1 with a fiducial cosmology at the best-fit parameters, and ℓ -range 2 – 2500. The left plot in Figure 6, shows the diagonal elements of the signal part and the noise part of C_ℓ , while the right one shows the KL-transformed eigenmode D_ℓ of C_ℓ . We can see that the first KL mode contains most of the SNR contribution to the power spectrum. However, if we want to recover more information, we also should include the second and the cross mode between the first and second KL-mode.

In Figure 7, we plot the normalised KL-eigenmode E_ℓ^i of C_ℓ and its corresponding $U_\ell^{ij} = R_\ell^i R_\ell^j$. Modes with different ℓ are plotted in increasing shades of the colour. We can see that the KL-modes do not depend significantly on the scale factor ℓ , so we also take the weighted average of the eigenmodes E_ℓ^p and its quadratic form W_ℓ over ℓ 's and plot them with black lines. We see that for different ℓ , the KL-modes do vary by a slight amount. For the first KL-mode, the tomographic bins with higher redshift gain more weight than those with low redshift. This is also shown by the weight on tomographic combination that the combination of bin 3 and bin 4 gains most of the weight to maximise the signal-to-noise ratio. This agrees with the fact that the diagonal elements C_ℓ for low redshift is much less than those with high redshift.

We perform KL-compression with the first mode and with the first two modes separately. In Figure 8, we plot the compressed covariance matrices for the CL and the Gaussian covariance with the first mode only, and show a one-to-one comparison of the covariance matrices. By comparing the bottom panel of Figure 2 with the left panel of Figure 8, we notice that the large regions containing the elements with greater difference are now gone. Instead, the two covariance matrices just have a relative constant difference, because of the fact that we did not include non-gaussian effect in one of them. This shows that the divergence between CL and the Gaussian covariance does not considerably affect the overall SNR.

We ran the likelihood analysis with the first KL-mode and the first two KL-modes, which correspond to a 10-to-1 and 10-to-3 compression, respectively, and show the parameter constraints on the $\Omega_m - S_8 - A$ plane in Figure 10. We can see in the figure that the first KL-mode is generally not enough to recover the information in the data vector. Since the first two modes contain most of the SNR contribution on the map level, we were able to recover the Ω_m constraints. However, the recovery on the S_8 and A is not desirable. This could be due to the fact that the SNR-prioritised modes are not the sensitive direction for these parameters, as was also the case in Figure 5. Indeed, the $S_8 - A$ plane shows a strong correlation between these two parameters. This could explain why the S_8 constraints got wider: the KL-modes fail to break the degeneracy on A , which is mostly contained in the modes that are insensitive to cosmic shear, and are discarded in the compression process.

B. Linear combinations of the data vector

The compression here takes place at the two-point level [18], with the compressed data vector containing linear combinations of the many two-point functions. In principle, this works with only N_p two-point functions where N_p is the number of free parameters, and each mode, or linear combination, contains all the information necessary about the parameter of interest.

For each parameter p_α that is varied, one captures a single linear mode

$$y_\alpha = U_{\alpha i} D_i, \quad (11)$$

where D_i are the data points and the coefficients are defined as

$$U_{\alpha i} \equiv \frac{\partial T_j}{\partial p_\alpha} C^{-1}_{ji}, \quad (12)$$

with T_j being the theoretical prediction for the data point D_j . An illustration of the matrix $U_{\alpha i}$ is shown in Figure 14, showing the weighting vector for parameters Ω_m , S_8 and A .

The now much smaller data set $\{y_\alpha\}$, which contains as few as N_p data points, carries its own covariance matrix, with which χ^2 can be computed for each point in parameter space. Propagating through shows that this covariance matrix is related to the original C_{ij} via

$$C_{\alpha\beta} = U_{\alpha i} C_{ij} U_{j\beta}^T. \quad (13)$$

In our case, our covariance matrix is 227×227 , while the number of parameters needed to specify the model is only 16, so $C_{\alpha\beta}$ is a 16×16 matrix. We have apparently captured from the initial set of $(227 \times 228)/2 = 25,878$ independent elements of the covariance matrix a small subset (only 136 in this case) of linear combinations of these 25k elements that really matter. If two covariance matrices give the same set of $C_{\alpha\beta}$, it should not matter whether any of the other eighty thousand elements differ from one another.

Ultimately, what matters is how well the likelihood does at extracting parameter constraints. Since most analyses assume a Gaussian likelihood, this boils down to how well the contours in parameter space agree when computing χ^2 using two different covariance matrices.

Figure 11 compares the constraints obtained for the compressed covariance matrix and data set with results from the full one. The two curves agree extremely well for the parameters shown: Ω_m , S_8 and A . This is also true for all the other cosmological and intrinsic alignment parameters, where their mean values agree at the 2σ confidence level. While the volume of the whole constrained parameter space does increase by about 13%, the constraints for most parameters are less than 4% broader, which shows that the information loss is negligible.

One relevant point in this analysis is at which point to take the derivative of each parameter. When we wish to

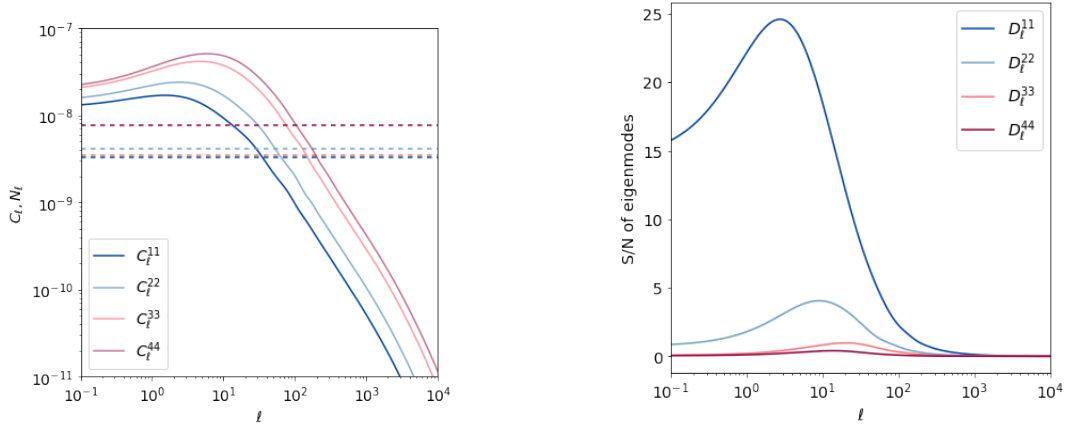


FIG. 6. **Left:** Shear power spectrum of CL. Solid lines are diagonal elements of the signal matrix S_ℓ , and dashed lines are the diagonal elements of noise matrix N_ℓ . **Right:** Signal-to-noise ratio matrix D_ℓ of KL-modes of the power spectrum on the left.

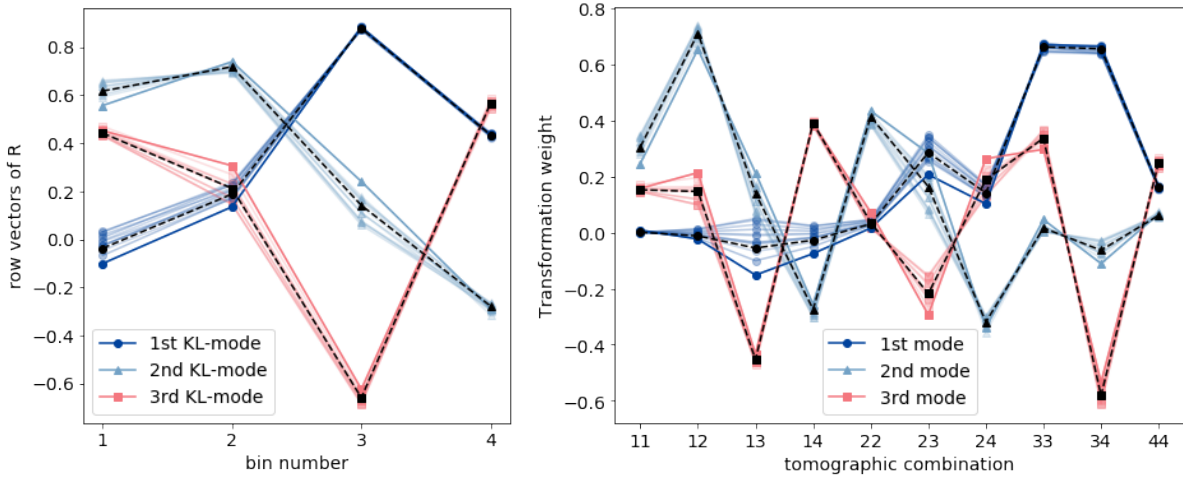


FIG. 7. **Left:** Normalised KL-eigenmodes E_ℓ^p of the shear power spectrum C_ℓ , the changes in shades represent different ℓ . **Right:** Transformation on tomographic bin combination W_{ij} constructed by the KL-eigenmodes. Black lines are the weighted average of each mode.

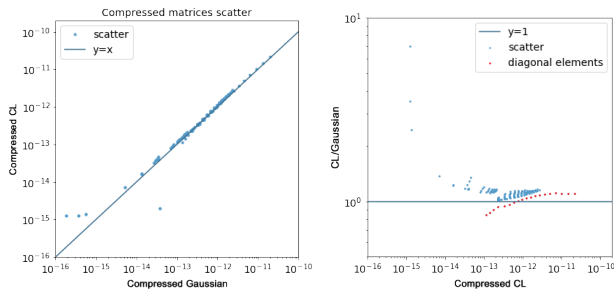


FIG. 8. **Left:** One-to-one scatter of the two compressed matrices following the procedure described in Section VIA. **Right:** One-to-one scatter of the ratio of CL over Gaussian and the CL elements.

important to derivate each parameter at their respective mean value (obtained by performing the analysis with the full covariance matrix). The shape and variance of the posterior is not dependent on the derivative, but the best-fit value shifts according to the point where the derivative is taken.

We also apply this methodology to comparing the covariance matrices of interest, i. e. CL and Gaussian. In order to do this, we take two different approaches: first, we assume that $U_{\alpha,i}$ is the same for both covariance matrices and we calculate it with CL. The second approach is that each compression scheme must use the original covariance matrix that will be compressed, so that $U_{\alpha,i}$ will be different for each covariance matrix. We find that the mean values of the parameter constraints for the two methods agree to 1σ , which shows that they are equivalent to each other. Figure 13 is obtained for the first method, which will be the one adopted from here on, it

compare the results of our compression scheme with those obtained with the full covariance matrix and data set, it is

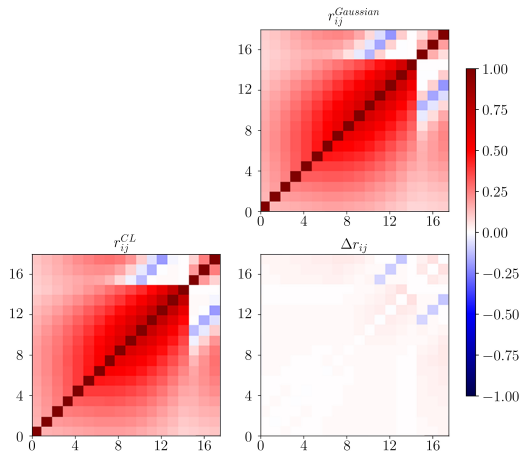


FIG. 9. The correlation matrix of Gaussian (upper right) and CL (bottom left) covariance matrices, and their difference (bottom right) in the elements

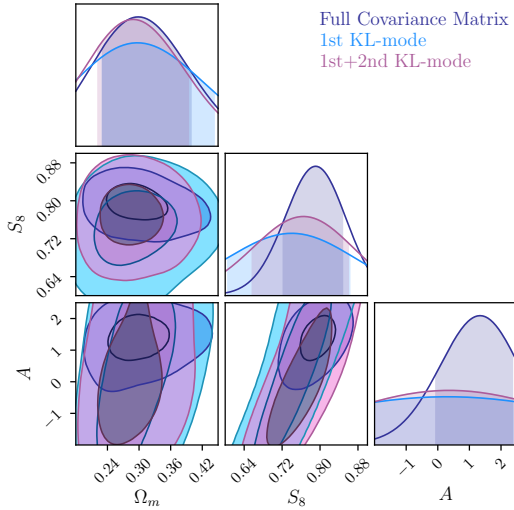


FIG. 10. Cosmological constraints marginalised over all 16 parameters for the 190×190 CL covariance matrix and that compressed by the first KL-mode and the first two KL-modes.

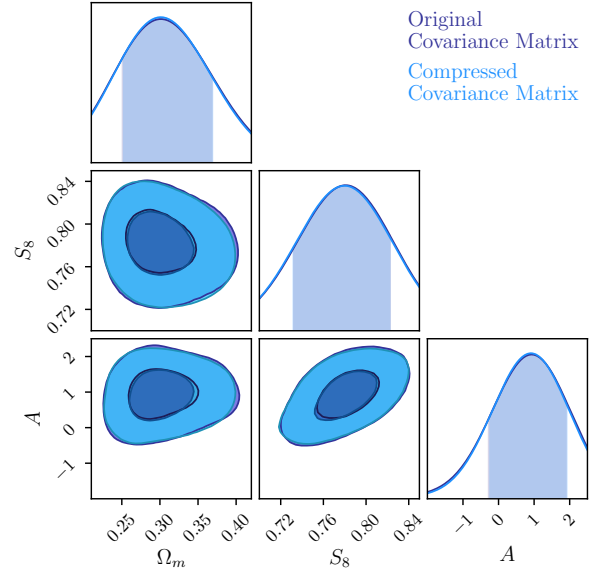


FIG. 11. Constraints on cosmological parameters Ω_m and S_8 and for the intrinsic alignment parameter A for the original CL covariance matrix (in purple) and for the compressed one (in blue).

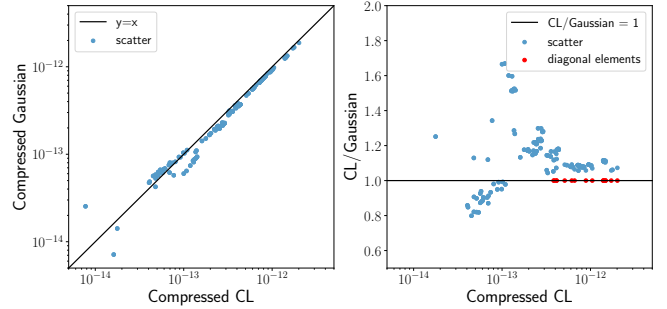


FIG. 12. **Left:** One-to-one scatter of the two compressed matrices following the procedure described in Section VI B. **Right:** One-to-one scatter of the ratio of CL over Gaussian and the CL elements.

VII. TOLERANCE OF THE COMPRESSED MATRICES

Now that we have shown that we are indeed able to compress the covariance matrix into a much simpler and considerably smaller one, our next step is to analyse the amount of error the elements can tolerate while reproducing compatible parameter constraints. In the next sections we test two different ways of perturbing the covariance matrix: first we consider an error to the elements themselves, and then we follow a similar procedure to study the effects of introducing error to the eigenvalues.

One of the issues that arises when arbitrarily modifying the elements of the covariance matrix is that the new one does not necessarily remain positive definite. In this analysis, we take an extra step to ensure that this

shows the correlation matrix for Gaussian and CL, and the difference between the diagonal elements. We find this figure important because we can clearly see the difference between the two matrices by simply looking at only $(16 \times 17)/2$ elements, as opposed to having to analyse the larger correlation matrix for the full covariance matrices. It is also crucial that the matrices used for comparison here are those obtained via the same compression scheme, so that we can be sure that their differences are indeed only related to the differences in the original matrices.

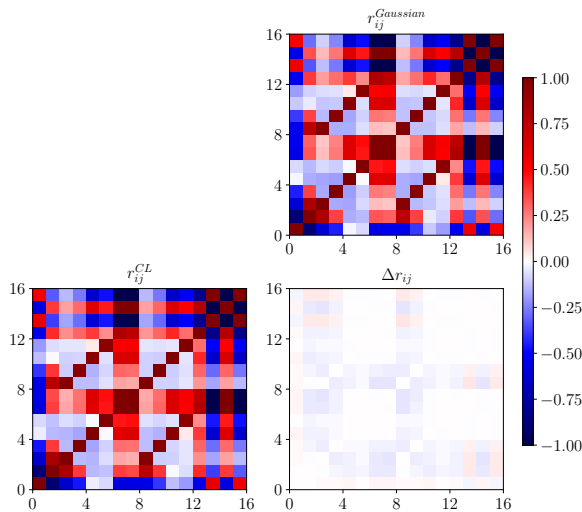


FIG. 13. The upper right and lower left plots display the correlation matrix for Gaussian and CL respectively, and the difference between them, Δr_{ij} , is shown on the lower right.

characteristic is retained.

A. Modifying the elements

To quantify the error tolerance of the elements of the covariance matrix, we introduce error in the following manner: consider that we want to test the impact of an error $x\%$; this can either be an increase or a decrease of the original element, such that what we care about most is not whether the parameter constraints will be larger, but rather how different. For this error to be random, but centred at our desired percentage, we draw δ from a Gaussian distribution, $\mathcal{G}(0, \frac{x}{100})$ and calculate the new value to be

$$C_{\alpha\beta}^{\text{new}} = (1 + \delta)C_{\alpha\beta}^{\text{old}}. \quad (14)$$

We keep the matrix symmetric by making $C_{\alpha\beta} = C_{\beta\alpha}$, and, finally, we check for positive definiteness. We show the constraints on Ω_m and S_8 in Fig. 15, in black, where the green rectangle spans over the constraints for the original covariance matrix. We see that errors of up to 25% translate to $< 10\%$ difference in the constraints. A 30% error, on the other hand, shows differences of up to 33% and 24%, respectively. It is worth noting here that we also find that S_8 is less sensitive to these noise introduced.

B. Modifying the eigenvalues

Another way of introducing error to the covariance matrix is to perturb its eigenvalues. For a symmetric matrix, we have

$$C_{\alpha\beta} = Q\Lambda Q^{-1}, \quad (15)$$

where $\Lambda = \lambda I$, with λ being the eigenvalues and I the identity matrix; and Q is a square matrix whose columns are composed of the eigenvectors of $C_{\alpha\beta}$. The eigenvalues are then perturbed as described in Eq. 14, with an extra step to guarantee $\delta > 1$, then $\lambda^{\text{new}} > 0$, thus keeping the matrix positive definite.

The results for this method are also plotted in Fig. 15, in blue, for Ω_m and S_8 . In general, we find that we are not able to reproduce significant changes to the parameter constraints, even with 30% errors, as the resulting constraints are all within 5% of the original one. As such, it is not clear that the results obtained using this procedure is equivalent to modifying the actual elements of the covariance matrix.

VIII. CONCLUSION

In this work we set out to explore efficient ways of comparing, analysing and compressing covariance matrices. We started off looking at the parameter constraints of two 227×227 covariance matrices CL and Gaussian, generated for DESY1 cosmic shear measurements, and saw that, although some of their elements differed by several orders of magnitude, they generated similar constraints. It was clear, then, that not all elements contribute equally to the parameter constraints, and we needed to employ increasingly complicated methods to try and locate the most relevant parts of the covariance matrix.

The first step was then to analyse the eigenvalues. We began with the hypothesis that modes associated with the lowest eigenvalues have the lowest variance and therefore carry most information, as such, those with the highest eigenvalues would contribute less to parameter estimation. This proved to be untrue: “removing” the highest 200 eigenvalues, by setting them to nine orders of magnitude higher resulted in a loss of about 200% on the constraining power. Next, we moved on to the signal-to-noise ratio, and, using a similar procedure adopted for the eigenvalues, we “removed” the modes with the lowest SNR. The results showed us that these modes did not contribute significantly to constraining some cosmological parameters, like Ω_m , but constraints on the intrinsic alignment parameters, and even S_8 were considerably affected. This is consistent with the fact that the IA parameters are more sensitive to low SNR, and it shows us that we need to look at the SNR per parameter before making any cuts, so that we do not lose important information for the parameters that we want to constrain.

Finally, we explored methods of shrinking the covariance matrix. We explored two such methods: a tomographic compression, and another directly on the two-point functions. For the first method, we decompose the shear power spectrum into KL modes, then we look for those with the highest SNR. We thus go from ten tomographic bins to only one or two. The consecutive covariance matrix, for one mode, is then reduced from

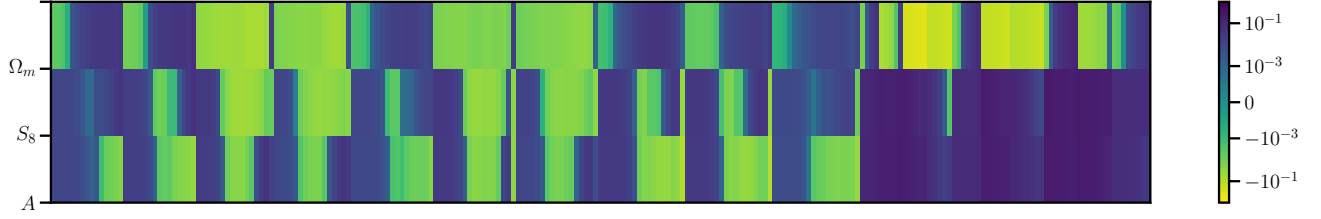


FIG. 14. An illustration of the 227 values of the weights corresponding to Ω_m , S_8 and A used for compressing the covariance matrices. Note how similar the weighing vectors for S_8 and A , and that the largest values for correspond to the last 60 elements, i.e. these will be used to compress the part of the covariance matrix that holds information for ξ_- .

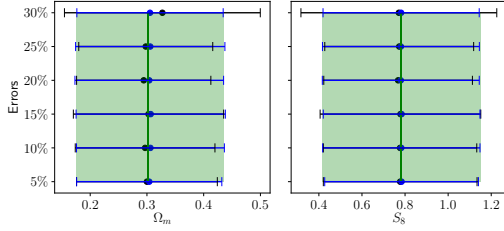


FIG. 15. An error plot showing the changes to the constraints for Ω_m and S_8 for errors added at 5%, 10%, 15%, 25% and 30% of the original elements (in black) and eigenvalues (in blue) of the compressed covariance matrix. The green rectangle englobes the 2σ interval obtained for the original CL covariance matrix, and the green line shows the mean value for the respective parameter.

correlation matrices being very similar, and the diagonal elements showing a percentage difference of less than 15%.

One last step was taken to analyse the error tolerance of the compressed covariance matrix. We first introduced random errors of 5%, 10%, 15%, 20%, 25% and 30% and found that the constraints are consistent with the original ones for an error of up to 25%; errors larger than that cause the constraints to increase. We also applied these errors to the eigenvalues of the covariance matrix, and found the differences in the constraints to be less than 3%, even for those larger than 25%.

Acknowledgments

The author wish to thank Sukhdeep Singh and Hung-jin Huang for useful discussions.

T.F. and T.Z. contributed extensively writing the main paper as well as implementing the covariance comparison and compression. N.C. contributed to the compression code. All authors participated in the discussion and gave valuable suggestions.

The DESC acknowledges ongoing support from the Institut National de Physique Nucléaire et de Physique des Particules in France; the Science & Technology Facilities Council in the United Kingdom; and the Department of Energy, the National Science Foundation, and the LSST Corporation in the United States. DESC uses resources of the IN2P3 Computing Center (CC-IN2P3-Lyon/Villeurbanne - France) funded by the Centre National de la Recherche Scientifique; the National Energy Research Scientific Computing Center, a DOE Office of Science User Facility supported by the Office of Science of the U.S. Department of Energy under Contract No. DE-AC02-05CH11231; STFC DiRAC HPC Facilities, funded by UK BIS National E-infrastructure capital grants; and the UK particle physics grid, supported by the GridPP Collaboration. This work was performed in part under DOE Contract DE-AC02-76SF00515. T.F. also acknowledges financial support from CAPES and FAPES.

- nomical Society, 473, 4306
- [3] Antony Lewis, Anthony Challinor, A. L. 2000, The Astrophysical Journal, 538, 473
- [4] Bellini, E., Alonso, D., Joudaki, S., & Waerbeke, L. V. 2019, arXiv:1903.04957
- [5] Bridle, S., & King, L. 2007, New Journal of Physics, 9, 444
- [6] Feroz, F., Hobson, M. P., & Bridges, M. 2009, Monthly Notices of the Royal Astronomical Society, 398, 1601
- [7] Gualdi, D., Manera, M., Joachimi, B., & Lahav, O. 2018, Monthly Notices of the Royal Astronomical Society, 470, 4045
- [8] Howlett, C., Lewis, A., Hall, A., & Challinor, A. 2012, Journal of Cosmology and Astroparticle Physics, 2012, 027
- [9] Joachimi, B. 2017, Monthly Notices of the Royal Astronomical Society: Letters, 466, L83
- [10] Kilbinger, M., Benabed, K., Guy, J., et al. 2009, Astronomy Astrophysics, 497, 677
- [11] Kirk, D., Rassat, A., Host, O., & Bridle, S. 2012, Monthly Notices of the Royal Astronomical Society, 424, 1647
- [12] Köhlinger, F., et al. 2017, Monthly Notices of the Royal Astronomical Society, 471, 4412
- [13] Krause, E., & Eifler, T. 2017, Monthly Notices of the Royal Astronomical Society, 470, 2100
- [14] Smith, R. E., Peacock, J. A., Jenkins, A., et al. 2003, Monthly Notices of the Royal Astronomical Society, 341, 1311
- [15] Takahashi, R., Sato, M., Nishimichi, T., Taruya, A., & Oguri, M. 2012, The Astrophysical Journal, 761, arXiv:1208.2701
- [16] Tegmark, M., Taylor, A. N., & Heavens, A. 1997, The Astrophysical Journal, 480, 22
- [17] Troxel, M. A., et al. 2018, Physical Review D, D98, 043528
- [18] Zablacki, A., & Dodelson, S. 2016, Physical Review D, 93, 083525
- [19] Zuntz, J., Paterno, M., Jennings, E., et al. 2015, Astronomy and Computing, 12, 45